Institut für Pharmazie, Fachbereich Chemie und Pharmazie der Johannes-Gutenberg Universität Mainz, Germany

A molecular modeling study of B-DNA-intercalation complexes with amsacrine and related 9-anilino-acridines

G. Fischer and U. Pindur

Computer molecular modeling studies of some complexes of amsacrine-derivatives with B-DNA-hexanucleotides were performed to shed new light on the DNA-binding mode of these drugs. The studies are based on routine methods, as are the semiempirical calculations, conformational analyses of the ligands, interaction field analyses, force field and molecular dynamics simulations of ligand/base paired DNA-complexes. The predictions suggest that the tested 9-anilino-acridines **1**, **3** and **4** bind by intercalation to the base-paired oligonucleotides. Depending on the substitution pattern of the tested 9-anilino-acridine-series compounds, some distinct binding modes and base sequence selectivities were observed.

1. Introduction

From the series of 9-anilino-acridines the drug amsacrine (**1**) was introduced as a drug for the therapy of acute myeloic and acute lymphatic leukemia (Fig. 1) [1, 2]. A newer analogue, the compound asulacrine (**2**), has been launched in phase I clinical trials for the treatment of lung and breast cancer [3, 24].

Amsacrine (**1**) and structurally related derivatives intercalate between the base pairs of the DNA and thus induce apoptosis of the tumor cells via topoisomerase II-inhibition [4–7]. A great variety of 9-anilino-acridines have been synthesized since 1976 and detailed structure-activity relationship studies have been performed including QSAR studies for a more rational molecule design [8–15, 24]. To complete these investigations some computer molecular modeling studies of complexes of amsacrine (**1**) with base paired DNA di- and tetra-nucleotides have been performed and some preliminary predictions of intercalation of the drug from the minor groove side of DNA are reported [16–19].

However, in order to get more information at the atomic level about the DNA-binding-mode of 9-anilino-acridines an extensive theoretical study including molecular dynamics aspects is justified. Extended molecular modeling studies involving appropriated program tools should be useful to rationalize the hitherto reported experimental results of structure-activity relationships. Moreover, to our knowledge, no crystallographic or NMR data concerning 9-anilino-acridine intercalation complexes exists and therefore for this series of compounds a rational drug design of new antitumor active compounds must be supported exclusively by computer molecular modeling investigations.

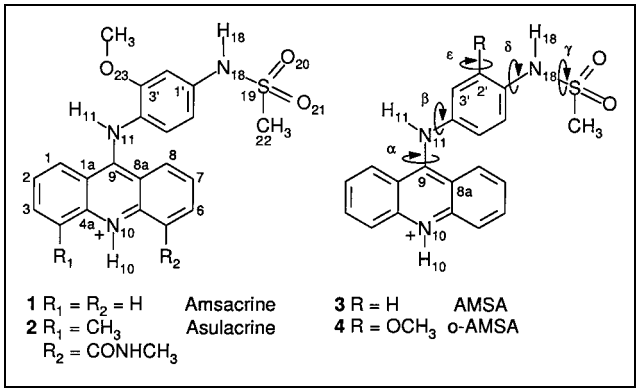

Fig. 1: The 9-anilino-acridines **1**–**4** with antitumor activity. The arrows indicate rotated bonds during the conformation analyses (chapter 2.2)

In continuation of our molecular modeling studies of intercalation complexes [20–22] we present some new interaction models of three 9-anilino-acridines **1**, **3** and **4** with particular B-DNA hexanucleotides. These models were based on crystal structures, on conformational analyses of the ligands, and on calculations of the interaction fields of B-DNA and some 9-anilino-acridines. They provided information about orientation modes of the ligand at the target. On the basis of these results molecular mechanics and some preliminary molecular dynamics simulations of the base-paired B-DNA-hexanucleotide/9-anilino-acridine complexes were performed. The given results should permit an extended design of new chemotherapeutic 9-anilino-acridine series congeners.

2. Investigations, results and discussion

2.1. Minimization of the ligands, validation

The crystal structures of the N10-(un-)protonated 9-anilino-acridines **1**, **3** and **4** were minimized by semiempirical quantum mechanical methods [57]. The quantum mechanically computed acridine moieties show RMS deviations of 0.06–0.16 Å from related crystal structures [53, 57] (and after force field minimization [53]). This RMS deviation is comparable with the RMS deviation between the crystal structures of the compounds, revealing 0.04–0.18 Å [45]. Therefore the calculated conformations are in good agreement with the crystal structure geometries.

2.2. Conformational analysis of the ligands

The miminized conformations of the 9-anilino-acridines **1**, **3** and **4** are starting points of the MOPAC/AM1 conformational analyses.

Amsacrine (**1**) and AMSA (**3**) revealed similar maxima and minima concerning the rotation of the bond C9–N11 (Fig. 1). In the N10-protonated form the free electron pair at N11 is in conjugation with the acridine ring. Thus, an energetically favored C9–$N11^+$ imino structure with a planar acridine ring gave rise to minimum conformations with a torsion angle α at about 0° or 180°. At about +/– 90° the conjugation is sterically prevented, so that N11 turns out to become pyramidal.

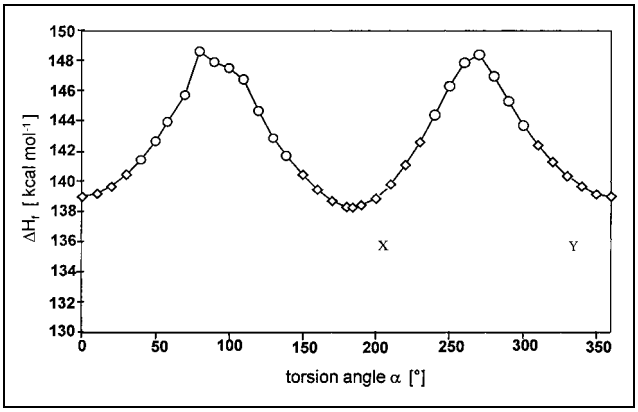

Fig. 2: MOPAC/AM1 quantum mechanical conformation analysis of the N10-protonated amsacrine (**1**). ΔHf vs. torsion angle α [C8a−C9−N11−C3′]. Planar conformations: rhomb, +/− pyramidal conformations: circles. X, Y: torsion angles of the crystal structures of N10-protonated 9-anilino-acridine derivatives, which are planar at N11 in full conformity with the corresponding calculated conformations [26, 76]

The minimum conformations of the acridines **1** and **3** show the ortho-methoxy group at the phenyl ring turned away from the acridine plane (*s-cis*-orientation of H11/OCH_3), fully compatible with the crystal structure geometries [12, 25, 27].

In contrast the methoxy group of the amsacrine derivative o-AMSA (**4**) adopts in the conformational minimum an *s-trans* orientation of H11/OCH_3, which is also formed in the crystal state [23].

In summary, the conformational simulations with MOPAC/AM1 at the C9/N11 axis predict the expected transition from the energetically favored planar, conjugated to the pyramidal conformation at the N11-amino group. The conformations of **1** correspond to the geometries of the X-ray crystal structures.

The geometry of the sulfonamide group is of special interest considering interactions in the DNA grooves. Therefore the conformation of this functionality was analysed separately by MOPAC/AM1 [57]. The calculated energetically mostly favored conformations are those which produce an hydrogen bond between an oxygen of the sulfonamide group and a nearby hydrogen atom of the phenyl ring. This result is in part an artefact of the calculations in vacuo, although hydrogen bonding with aromatic hydrogens is observed in some crystal structures [43, 44].

Furthermore a CSD search for validation of the partial structure C−C−N−SO_2−CH_3 was performed [55]. These studies revealed three conformational families relating to the torsional angle C1′−N18−S19−C22 (Fig. 3).

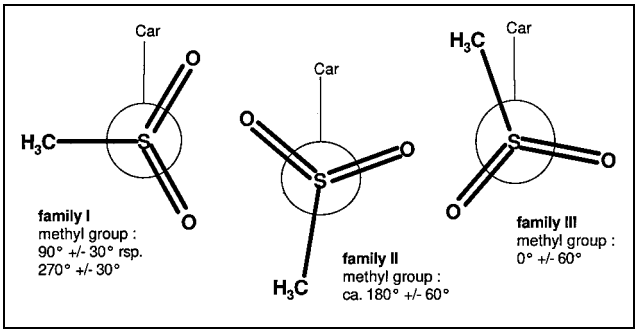

Fig. 3: Newman projections of the conformational families of the C−C−N−SO_2−CH_3 partial structure, CSD search (Car = carbon of the aromatic ring) [55]

According to the results of the CSD-search [55, 79] the families II and III were each represented by 4 and the family I by 20 crystal structures. The position of the substituents in the family I is apparently energetically favored in the solid state.

The molecular mechanics calculations of the protonated acridines **1**, **3** and **4** favor the conformation types I and II. Family III is energetically disfavored in the force field calculations for steric reasons. The MOPAC/AM1 conformational analysis for the family I in the 9-anilino-acridines is energetically favored.

The molecular dynamics simulations (vide infra) of the intercalation complexes revealed that the side chain of the 9-anilino-acridines adopts mainly conformations I or II. With this result in mind, crystal structures with hydrogen bonds to the sulfonamide group (N−H . . . N-type) were conformatively analysed [55]. All of the 22 found CSD conformations exhibiting intra- or intermolecular hydrogen bonds did exist in the conformational type I.

In summary, the quantum mechanical and the force field conformational studies concerning the sulfonamid-group either free or in complexes with a hydrogen bond predict conformations as found in the crystal state.

2.3. B-DNA-hexanucleotide construction and minimization

A DNA-hexanucleotide with a central intercalation cavity was chosen in order to simulate the *in vivo* situation as found in a longer DNA-fragment, because the side chain of the 9-anilino-acridines is able to interact with the neighbouring two base pairs in a groove after intercalation of the acridine moiety between the DNA base pairs.

To construct B-DNA-hexanucleotides with a central enlarged intercalation cavity the crystal structure of daunomycin/d**CG**CG**CG**/formaldehyde [28] was used. (For abbreviations see [80]). According to the schematic presentation in Fig. 4, two molecules of the base paired d**CG**CG**CG** were superposed, all base pairs except BP3′ and BP4′ or BP3″ and BP4″ were eliminated. As an appropriate CG-unit the $r(CG)_2$ base pairs of the ethidium/rCG crystal complex was introduced [29]. After deletion of the double atoms (doubled due to the formal fit of one molecule onto another molecule) and the 2′-hydroxy groups of the D-ribose unit, the molecules were combined covalently to give rise to the new B-DNA hexanucleotide with an enlarged intercalation cavity in the centre of the molecule (Fig. 4).

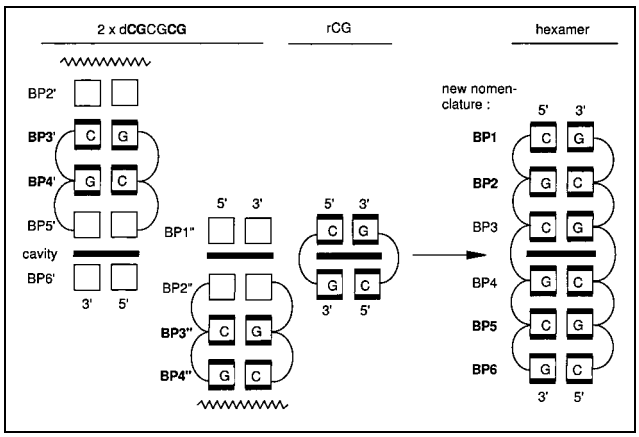

Fig. 4: Construction of the DNA-hexanucleotide by a superposition/deletion strategy, starting from two d**CG**CG**CG** crystal structure fragments [21, 28, 29]. Bows indicate the phosphate backbone fragments used for the new molecule

For the variation of the sequence of this hexanucleotide the bases BP3, BP4 and BP5 were exchanged against planar A/T or C/G base pairs. The appropriated AT base pair was taken from the crystal structure of dCGATCG [30]. The minimization process for the constructed hexanucleotides is described in chapter 3.3.

2.4. Interaction field analysis with the program GRID

For prediction and analysis of the preferred molecular/atomic interaction positions special programs are used, which are already successfully applied in CoMFA or 3D-QSAR studies [31]. In our hands the program GRID, version 9.02 [32], was applied to the simulation of non-covalent interactions between a ligand and the biopolymer target DNA. In GRID simulations the force field energies between a target molecule and the so-called probe were calculated in a defined three-dimensional segment. For the discussion of relevant interactions the shapes of the isoenergy contour fields are compared. They depend on definitive steric and electrostatic effects.
Several GRID-probes were chosen to get detailed information about the DNA-sequence specificity, the preferred orientations of the acridine moiety in the intercalation cavity and the side chain in the grooves. The applied probes are adapted to the structural features of **1** (see Fig. 5). Fig. 6 shows details of the DNA.

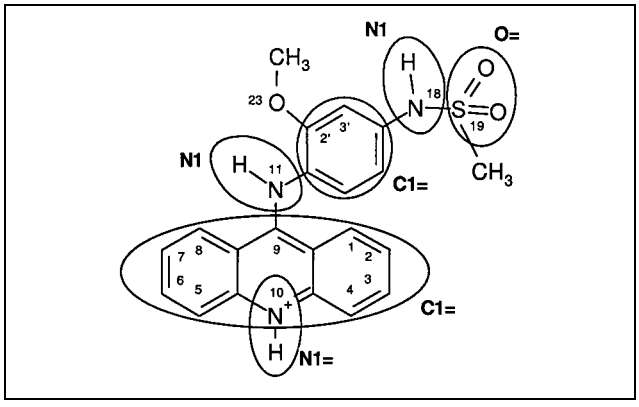

Fig. 5: With the exception of the water probe the GRID probes were orientated at the amsacrine drug (**1**). Parametrisation and a short characterisation of the probes introduced in this paper are given in Table 1, chapter 3.4 [33]

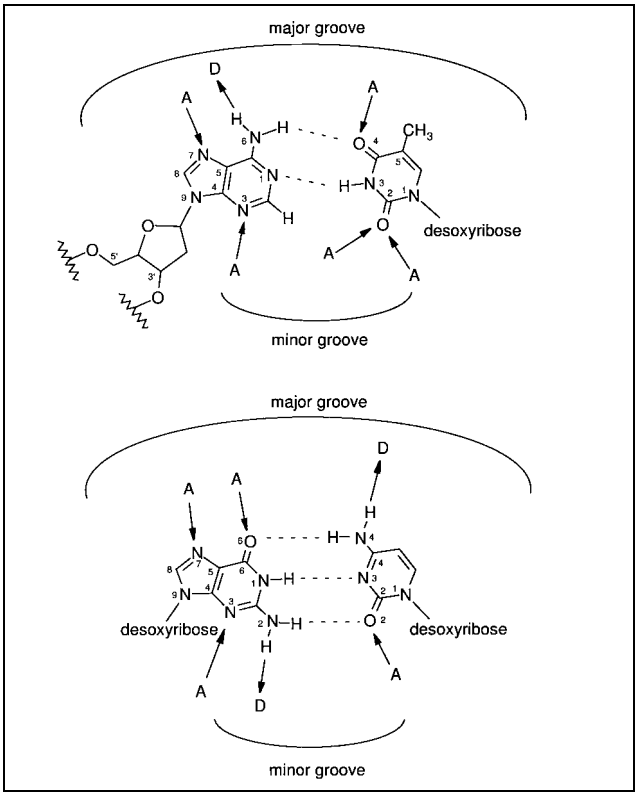

Fig. 6: B-DNA bases and the sugar phosphate backbone with acceptor (= A) and donor (= D) functions [63, 73]. Upper part: A*T with a partial structure of the backbone, lower part: G*C

2.4.1. GRID analyses of the B-DNA cavity

These GRID calculations should shed light on the possible preferred binding orientations of an intercalator within the intercalation cavity.

The aromatic probe C1=

The aromatic probe C1= is capable to detect favorable interaction sites for an aromatic moiety in the DNA cavity. In the case of dCG**C**G**C**G the energetically favored, broad intercalation field is positioned symmetrically between the stacked base pairs (Fig. 7), fully compatible with the results of crystal structures [62].
A clear difference between the C/G and A/T cavities is given. The calculations with the C1= probe concerning the sequence dCG**AT**CG revealed a smaller band with

Table 1: Parametrisation and short characterisation of the GRID probes used [33]

Probe	N1=[a]	N1[b]	O=[b]	C1=[a,b]	OH2[a,b]
VDWR[c]	1.65	1.65	1.60	1.90	1.70
EFFN[d]	7.0	7.0	6.0	6.0	7.0
ALPH[e]	1.80	1.40	2.14	2.07	1.20
CHARGE[f]	0.660	−0.080	−0.400	0.000	0.000
JD/JA[g]	1/0	1/0	0/2	0/0	2/2
EMIN[h]	−2.00	−2.00	−4.00	0	−4.00
RMIN[i]	1.60	1.60	1.40	0	1.40
TYP and comment	sp^2-amine: NH cation; protonated acridine-N10	planar NH; sulfonamide- or sec. Aminogroup of amsacrine	sulfonamide-oxygen	aromat. sp^2-C with H; acridine in the cavity	water; turned to get the maximum of possible H-bonds

Selection orientated at amsacrine (**1**), Fig. 5
[a] Used in the intercalation cavity.
[b] Used in the B-DNA-grooves.
[c] Van der Waals radius of the probe [Å].
[d] Number of effective electrons surrounding the probe.
[e] Polarizability of the probe [Å · kcal^3].
[f] Electrostatic charge on the probe [eV].
[g] Maximum number of hydrogen bonds which the probe group can **d**onate (JD) and accept (JA).
[h] Energy value at the energy minimum of the hydrogen bond function [kcal mol^{-1}]. Bonding angle: parametrized with the type of probe (independent from EMIN).
[i] Hydrogen-bonding radius of the probe [Å].

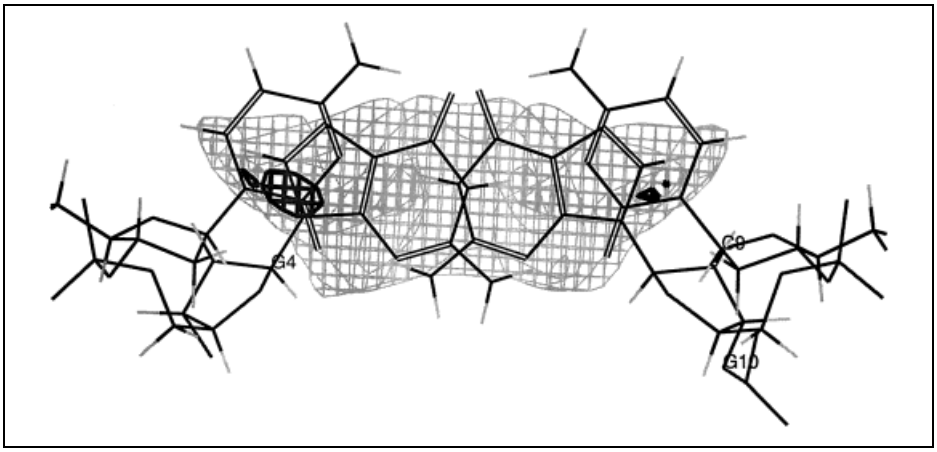

Fig. 7:
Intercalation cavity of dCG**CG**CG, probe C1=, top view. The optimal position of an aromatic intercalator parallel to the base pairs (edge on alignment) is obvious. Isoenergy contour field coding: bold lines −4.2, grey lines −3.0 kcal $\cdot$ mol^{-1}

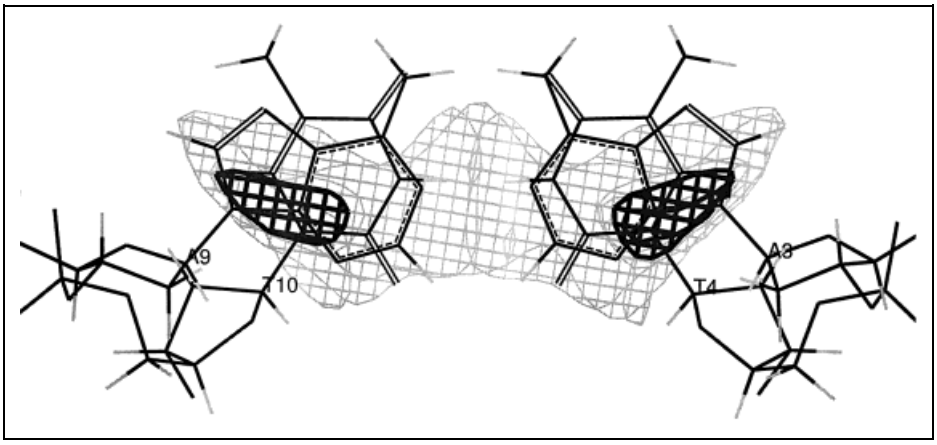

Fig. 8:
Intercalation cavity of dCG**AT**CG, probe C1=, top view. The interaction field is much smaller than that of dCG**CG**CG, see Fig. 7 and text. Isoenergy contour field coding: bold lines −4.2, grey lines −3.0 kcal mol^{-1}

bays and more extended decentral maxima of the interaction fields positioned close to the backbone (Fig. 8). If a DNA-substructure as thymine together with its part of the backbone is studied on its own, the calculations with the aromatic probe lead in this case to the compact decentral interaction fields in the cavity (Fig. 8).
Moreover several other DNA hexanucleotides with variable base pairs BP3 and BP4 were calculated. For example dCG**AA**CG, dCG**TT**CG and dCG**CT**CG revealed strong asymmetric fields located "beyond" the Py-bases. In this case an intercalation parallel to the base pairs (edge on alignment position of the chromophore) should be energetically less favored.

The probe N1= as hydrogen bond donor

The probe N1= as a hydrogen bond donor was used (Figs. 5, 6) to get information about the best position of the protonated N10 of the 9-anilino-acridine system. When AMBER charges are applied, the isocontour plots indicate strong field contributions in the center of the intercalation cavity of dCG**CG**CG and "beyond" the guanine bases in the cavity – as presented on the top view in Fig. 9.
In spite of the decentral maxima in combination with the backbone influence (Figs. 7, 8) there exists a significant energy gain for an NH^+ intercalator positioned in the central dCG cavity. When looking into the cavity from the front (base pairs perpendicular to the plane of view), relatively high intercalation bands can be seen, which offer incompletely planar intercalators a relatively high freedom for the energetically favored intercalation.
In the case of dCG**AT**CG some small interaction fields with a maximal gain of energy are nearly centrally located. Therefore a 9-anilino-acridinium drug is assumed to intercalate preferably in the center of the cavity.

In summary the GRID interaction fields suggest that with the exception of dCG**PuPu**CG and dCG**PyPy**CG an intercalation of an acridine moiety in the cavity parallel to the base pair planes and in an edge on alignment orientation seems energetically favored, locating the protonated N10 in the central region.

2.4.2. GRID analyses of the B-DNA grooves

There exists a variety of natural products and antitumor active drugs which act mostly in a sequence selective manner with one of the DNA-grooves or possess multibinding modes of action [21, 37, 50, 59]. The factors of molecular recognition of DNA grooves are represented by selective hydrogen bonds, van der Waals forces and hydrophobic and electrostatic contacts with the functionality on the "groundfloor" and at the "edges" of the DNA helix [22, 73].
Therefore studies of the three-dimensional, electrostatic characteristics of the DNA-grooves with GRID should give rise to information about base sequence selectivity, which is essential for the molecular recognition [21, 50, 60, 63]. The simulations should also give information about the optimal orientation of the side chain of the 9-anilino-acridines, reflecting interactions at the atomic level in the grooves [32]. The characteristic DNA donor/acceptor functions relevant for drug interactions are presented in Fig. 6.

2.4.2.1. GRID analyses of the major groove

Gene regulating enzymes prefer gliding along the broader and more functionalized major groove [64–66]. It presents more information to a groove-reading enzyme because of its acceptor/donor sequences (major groove "AAD" or "DAA" for C*G or G*C and "ADA" for A/T vs. minor

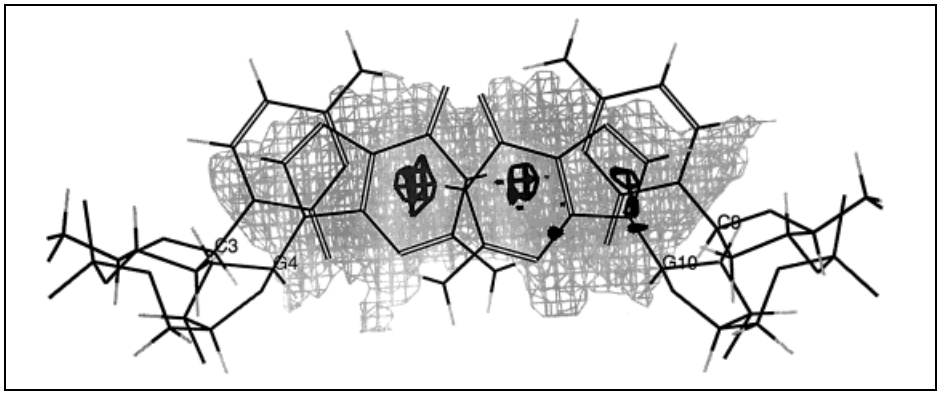

Fig. 9:
Intercalation cavity of dCG**CG**CG, probe N1=, top view. The optimal position for an N10-protonated acridine-N is slightly beside the middle of the cavity beyond the 6-membered rings of the guanine bases. Isoenergy contour field coding: bold lines −22, grey lines −10 kcal $\cdot$ mol^{-1}

groove "AAA" for A/T and "ADA" for C/G, Fig. 6). Therefore analysing the interaction fields in the grooves is worthwhile, though it was noted, that amsacrine also intercalates from the major groove to enter the ternary complex with topoisomerase IIα [64, 68].

The probe O= as hydrogen bond acceptor

The probe O= simulates a sulfonamide-oxygen as in the amsacrine derivatives (Fig. 5). The formation of hydrogen bonds between drug and major groove to the bases Ade-HN6 and Cyt-HN4 as donors is possible (Fig. 6). The 5′-BP_xBP_{x+1}-3′ base sequences dAG, dCG, dTG, dGG and dGT show at −4.5 kcal mol^{-1} interaction fields (Fig. 10), which are linked coherently and thus overlap several base pairs (at least 2). A sequence selective binding of a drug is therefore possible because of the directive effect towards these fields.
Especially with G*C as BP_x widely extended and energetically favored fields are produced as compared with other base pairs. The optimum is reached for BP_{x+1} with a cytosine in the B-strand (as G*C), because in this sequence a broad, overlapping 5′-BP_xBP_{x+1}-3′ GRID interaction field for dAG, dCG, dTG or dGG is formed.

The probe N1 as hydrogen bond donor

The GRID probe N1 (a planar NH amino group, simulating N11-H11 of the amsacrine derivatives, Fig. 5) should be able to form a hydrogen bond with the lone pairs of Thy-O4, Gua-O6, Gua-N7 and Ade-N7 (Fig. 6).
Around Gua-N7/-O6 a great coherent field develops and about Thy-O4 and Ade-N7 an oval field is formed. GRID shows that a maximum of energy gain is given in the distance of 2.8–3.1 Å revealing a hydrogen bond to the O atoms.

2.4.2.2. GRID analyses of the minor groove

In general the group of DNA ligands like the molecular small drugs prefer to bind to the minor groove of the B-DNA, because more intensive interactions are possible [48, 50, 60, 63]. Moreover the spine of hydration in the minor groove, especially in the AT rich sequences, favors drug binding in the context of an entropy driven interaction [48, 50, 73]. In the minor groove the base pairs A/T possess only acceptor functions ("AAA", Fig. 6), in contrast to the C/G base pair ("ADA", Fig. 6). Moreover for AT sequences a high charge density in the minor groove is characteristic [37, 67].

The probe O= as hydrogen bond acceptor

Hydrogen bonds are possible with the Gua-HN2 and should be marked by the probe O= (Fig. 5, 6). The calculations revealed a gain of energy of −5.2 kcal mol^{-1} for an isolated guanine (in the base plane to Gua-HN2) and up to −7.3 kcal mol^{-1} for the overlap area between dCG-dimers; see Fig. 11. Thus an optimal interaction is given for the dimer 5′-dCG-3′.

The probe N1 as hydrogen bond donor

In the minor groove many hydrogen bond acceptors exist together in a narrow room (Fig. 6). Using the probe N1 as a hydrogen bond donor (neutral amino NH-group, Fig. 5) the magnitude of the interaction fields of the bases decreases as expected: Thy-02 (two free electron pairs) > Cyt-02 (one free electron pair) > Ade-N3 = Gua-N3 (Fig. 12). The GRID fields of the bases are expanded partly into the fields of the backbone.
In summary, the N1 probe of GRID calculations revealed that A/T sequences are more favored than C/G sequences;

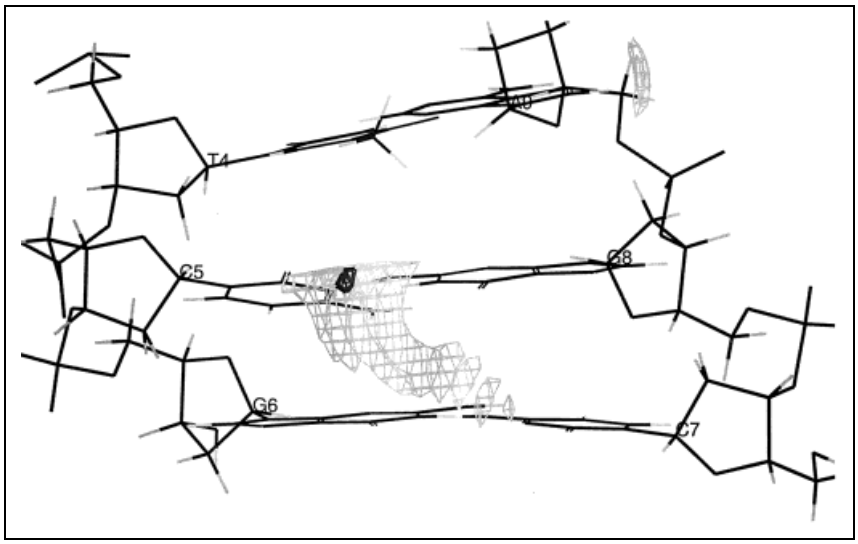

Fig. 10:
Major groove of dCG**AT**CG, probe O=, front view, BP4-6 are pictured. It's an example of broad base-pair overlapping fields in the major groove. The field reaches from Cyt-HN4 of C5 (in the middle) to Cyt-HN4 of C7 (lower right). The maximum (bold lines) is the optimal position for an acceptor to build a hydrogen bond to Cyt-NH4 of C5. The interaction field to Ade-HN6 (upper right) is isolated at the chosen energy value of −4.5 kcal mol^{-1}. Isoenergy contour field coding: bold lines −6, grey lines −4.5 kcal mol^{-1}

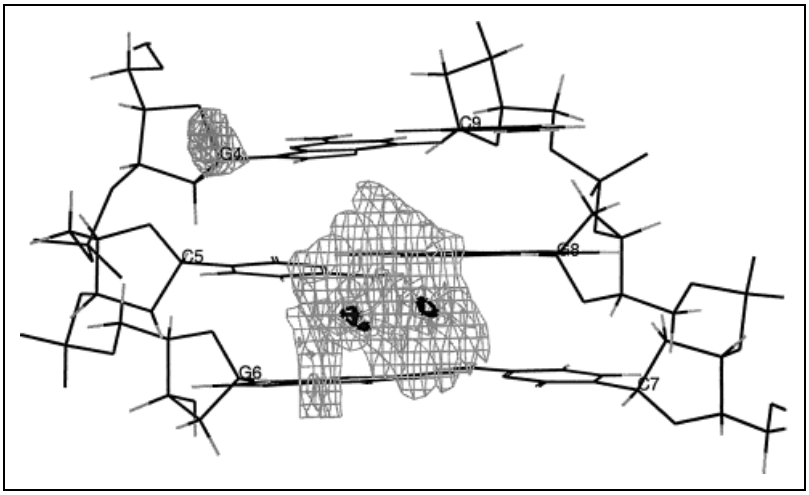

Fig. 11:
Minor groove of dCG**CG**CG, probe O=, front view of BP4-6. The central area between the base pairs C5*G8 (central) and G6*C7 (lower) is favored, because both fields of the G6- and G8-HN2 overlap. Moreover, if the probe is set in this position, it can bind additionally at both donor atoms, as for example with the sulfonamide-oxygens. Isoenergy contour field coding: bold lines −6, grey lines −4.5 kcal mol^{-1}

A/T-sequences produce, by the three point acceptor sequence "AAA", coherent interaction fields inside a base pair (Fig. 12). Thus drugs with groups of selectively localised hydrogen-bond donors will preferably "read" the floor of AT rich minor grooves for a maximum gain of interaction energy.

The water probe OH2

The application of the probe OH2 simulates the preferred spine of hydration in AT-rich sequences in comparison with the discontinuing interaction fields of GC-sequences. This is fully compatible with results from a variety of crystal structures [48, 73].

2.4.3. Summary and conclusions of the GRID calculations for the prediction of selective DNA interaction

• The acridines are anellated aromatic systems. GRID indicates, that an "edge on alignment" intercalation of the acridine moiety parallel to the planes of the base pairs into the enlarged DNA cavity seems possible. The N10 of the acridine ring can adopt an energetically favored central position in the cavity in both the protonated and the deprotonated forms.
5′-PuPu-3′ or 5′-PyPy-3′ sequences lead to asymmetrical fields mainly beyond the Py-bases, favoring a perpendicular intercalation – which is sterically prohibited for the amsacrine derivatives due to the 9-anilino – side chain.
• Water molecules exhibit donor and acceptor properties. GRID predicts well the experimentally proven hydration of AT sequences in the minor groove [48, 50, 73].
• With the program GRID valuable predictions of the orientation of the side chains of the 9-anilino-acridines in the grooves are possible. The calculated interaction fields reflect mainly the expected electronic and steric demands of the acceptor and donor functions. Moreover the results reflect the dimensions relating to space, overlap and additive interaction of these fields.
The major groove: The methoxy- or the sulfonamide O-atoms as acceptor functions can build up hydrogen bonds with Ade-HN6 or with Cyt-HN4. First of all dXG-dinucleotides like dCG produce optimal interaction fields.
The amino functions as donor functions of the ligands show no sequence selectiviy towards Pu-N7 or Thy-O4. Therefore only a trifling preference of dXG, dGX. dTX and dXT is observed.
The minor groove: On one hand C/G sequences are disfavored due to the steric effect of the Gua-NH2 group. This sequence destabilizes the intercalation of the acridine ring by dragging it out of the cavity as well as revealing incoherent interaction fields ("ADA" functions, Fig. 6).
On the other hand hydrogen bonds between the sulfonamide group and Gua-NH2 or between the amino groups of the 9-anilino-acridines and especially Cyt-O2 can be formed in the minor groove (ligands with acceptor function). The GRID calculations predict the affinity of ligands with an acceptor function to G/C sequences, which is verified by experimental methods, for example NMR spectroscopy [46, 48, 58-60] and in special cases by alkylation reaction of some ligands at Gua-N7 [61]. Other calculations gave similar results [22, 37, 46].
A/T sequences lead to coherent interaction fields in the whole minor groove. Replacement of water molecules from the minor groove is related to an entropy driven ligand binding. The NH partial structure of HN11 and of the sulfonamide can be involved in hydrogen bonds to the acceptor atoms of the AT bases.
Ligands with donor functions favor AT enriched minor grooves: dXT, dXA, dAX (X = each base pair possible), which is also verified in the literature [48, 50, 60, 73].
Base pair selectivity in the minor groove by ligands with acceptor functions is observed while studying the interaction fields of dCG, dXG or dCX versus dGC or A/T dimers: the first duplex types lead to broad, energetically favored interaction fields versus the small or not coherent fields of the dGC or A/T sequences. Moreover the GRID simulations favor the interaction with dCG more than with dCC, which is also experimentally supported [46, 59–61].

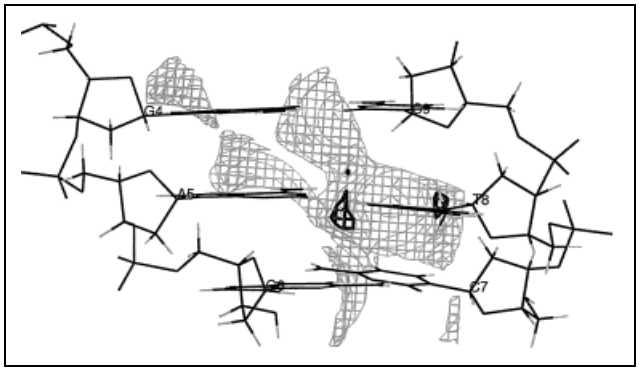

Fig. 12: Minor groove of dCG**CG**AG, probe N1, front view of BP4-6. The preference for AT (middle) can be seen in this isoenergy contour field. The optimum of hydrogen bond interaction points to the two free electron pairs of Thy-O2, and a great overlapping field around BP4/BP5 can be observed. Isoenergy contour field coding: bold lines −5.5, grey lines −4 kcal mol^{-1}

2.5. Simulations of 9-anilino-acridine/DNA-complexes by molecular dynamics simulations, molecular mechanics and semiempirical MO calculations

2.5.1. Molecular dynamics simulations (MD)

A preliminary molecular modeling study of complete DNA-drug complexes was performed in order to supplement the interaction field analysis (chapter 2.4). The molecular dynamics simulations were used to detect multiple local minima [31, 56]. Thus the configuration space of the intercalation complexes was scanned starting from a geometry with the intercalator set in 13 Å distance from the "edge" base pair-atoms of the hexanucleotide cavity (Fig. 13). This procedure was developed successfully in the literature [38]. The MD calculations were run with SYBYL [53], see chapter 3.5.1.

This arrangement of DNA and intercalator is heated periodically to 500 K and cooled to 50 K (MD **IA**, Table 2, chapter 3.5.ff.). The DNA is kept fixed. Similar MD simulations with successful results are reported by Fantucci et al. [56]. By heating to 500 K the intercalator gets enough kinetic energy to be able to migrate towards the DNA on the basis of electrostatic attraction. During the 50 K sessions molecular recognition between DNA and intercalator takes place. Thus this method should provide great advantages over former simple molecular mechanics methods for generation of intercalation complexes [16–19].

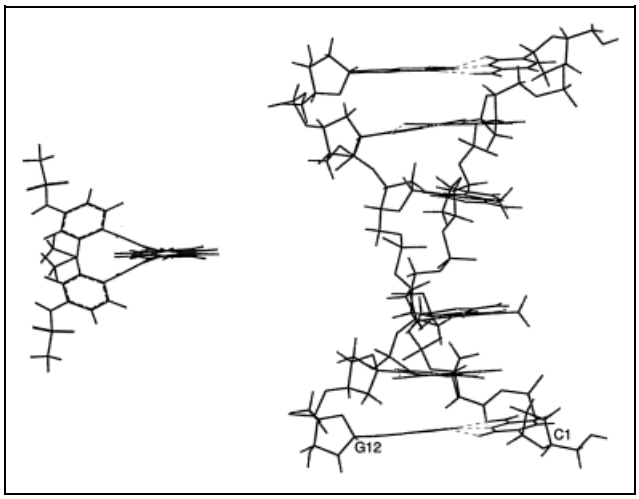

Fig. 13: Two superposed starting conformations of N10-protonated amsacrine (**1**) in front of the base paired dCG**AT**CG (start – MD **IA**, see text)

After partial or full intercalation or after the arrival on the surface of the DNA (outside complexes), another heating-cooling cycle is started, the so-called refinement MD **IB** (Table 2) [56]. In the case of partially intercalated drugs this following MD gives rise to fully intercalated complexes in most cases. Further on the conformational freedom of the complexes is checked and energetically favored conformational families can be found. This phase can be called the step of molecular recognition at the atomic level.

After optimization of outside and intercalated complexes (method **II**, chapter 3.5.2) minima were obtained for comparison, see Fig. 14.

The energetically favored intercalation complexes with the side chain lying in the minor groove are characterized by a nearly full intercalation of the acridine (top view, Fig. 14) in a small angle relative to the long axis of the base pairs of the cavity.

Intercalating into a dAT-cavity from the minor groove side often shows the hydrogen bond ligand-HN11 . . . Thy-O2 as predicted by the interaction fields calculated by GRID (probe N1, Figs. 6, 12, 14). Intercalation into a dGC-cavity from the minor groove side leads often to the hydrogen bonds ligand-HN11 . . . Gua-N3 or ligand-HN11 . . . Cyt-O2.

On the basis of the calculated potential energies some energetical relationships can be discussed (Fig. 15). The contact of the 9-anilino-group with the narrow minor groove is energetically favored throughout because of better van der Waals-contacts compared to the major groove (Δ 4.9–15.1 kcal mol^{-1} respectively) [17, 19, 73, 74]. By intercalation from the minor groove side the dAT-cavity

Table 2: Molecular dynamics simulation cycles [38, 56]

no.	Length (fs)	Step interval (fs)	Snap-shot (fs)	Temp. (K)	Temp.-coupling (fs)	Tolerance (Å)	Non-bonded contacts update (fs)
Method IA: start MD with 13 Å distance between DNA and ligand (length 16.9 ps)							
1/3	3000	1	500	500	10	0.0001	1
2/4/6/8/10	2000	1	500	50	10	0.0001	1
5/7/9	300	1	300	500	10	0.0001	1
Method IB: refinement MD of full or partial intercalated complexes (11.8 ps)							
1	600	1	600	500	10	0.0001	1
2/4/6/8/10	2000	1	500	50	10	0.0001	1
3/5/7/9	300	1	300	500	10	0.0001	1

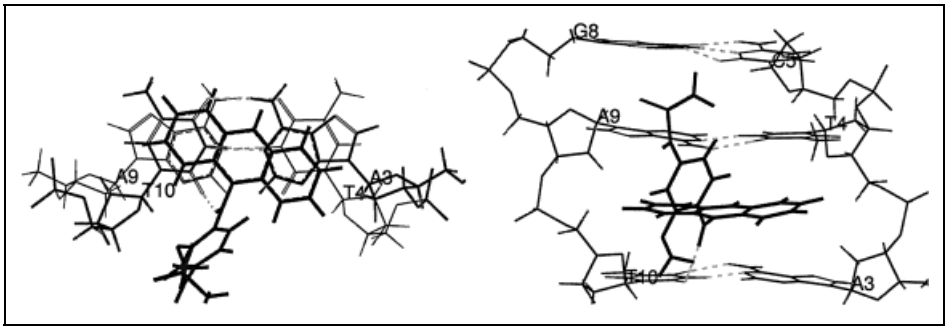

Fig. 14:
Energetically lowest complex of the N10-protonated amsacrine (**1**) intercalated into dCG**AT**CG, left side: top view of the dAT-cavity (base pairs and acridine parallel to the plane of view), right: front view of BP3–5 (base pairs perpendicular to the plane of view). The side chain is lying in the minor groove, showing the hydrogen bond from ligand-HN11 to Thy-O2 as predicted by the GRID interaction fields (Figs. 1, 12). See text. Hydrogen bonds: broken lines, intercalator: bold lines

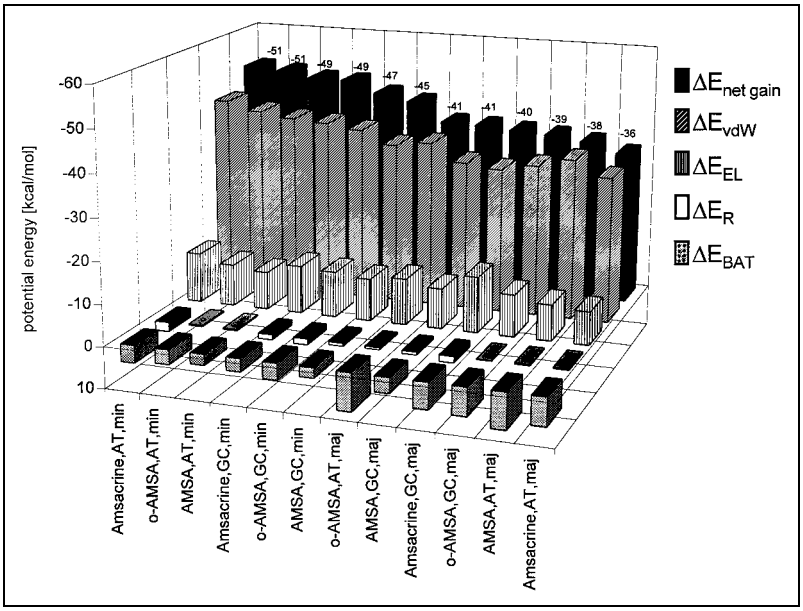

$$\Delta E_{net\ gain} = \Delta E_{vdW} + \Delta E_{El} + \Delta E_{R} + \Delta E_{BAT}\ [kcal\ mol^{-1}]$$

$$\Delta E_{vdW} = \Delta E_{van\ der\ Waals\ interactions} = E_{vdW\ complex} - E_{vdW\ DNA} - E_{vdW\ ligand}$$

$$\Delta E_{El} = \Delta E_{electrostatic\ interactions} = E_{El\ complex} - E_{El\ DNA} - E_{El\ ligand}$$

$$\Delta E_{R} = E_{R\ complex} - E_{R\ DNA} - E_{R\ ligand}$$

$$E_{R} = E_{out\ of\ plane\text{-}bending} + E_{1-4\ van\ der\ Waals\ interactions} + E_{1-4\ electrostatic\ interactions}$$

$$\Delta E_{BAT} = E_{BAT\ complex} - E_{BAT\ DNA} - E_{BAT\ ligand}$$

$$E_{BAT} = E_{conformational\ energies} = E_{bond\ stretching} + E_{angle\ bending} + E_{tosional\ strain}$$

Fig. 15: Survey of the potential force field energy and the partial terms Δ [kcal mol^{-1}] of the intercalation complexes of the N10-protonated amsacrine **1**, **3** and **4**. The DNA hexanucleotide dCG**AT**CG (= **AT**) and dCG**GC**CG (= **GC**) are fixed during the calculations, the side chain is lying in the minor (min) or major (maj) groove. Stabilizing energy contributions yield negative values (upwards columns). Destabilizing contributions to the total energy yield positive values (downwards columns). Energies are calculated according to the TRIPOS force field [53], see equation (3), chapter 3.5.2

of dCG**AT**CG is slightly (amsacrine, **1**) up to clearly (o-AMSA, **4**) favored.
In the major groove the interaction of the 9-anilino-group at the dGC-cavity of dCG**GC**CG is favored by **1** and **3** (Fig. 15). o-AMSA (**4**) again favors intercalation into the dAT-cavity from the major groove side of dCG**AT**CG. Amsacrine (**1**) even shows no base pair selectivity in experimental binding studies with DNA [51, 64, 69].
The ligands are forced out of their minimum conformations to fit into the intercalation cavity. This energy difference due to the induced fit yields Δ 4.9–7.3 kcal mol^{-1}. This energy range is fully compatible with citations in the literature [31], and according to that the geometries of the intercalated conformations are said to be thermodynamical stable.

Correlation with experimental data

No experimental thermodynamic data of amsacrine-DNA complexes are so far available in order to correlate the calculated values of $\Delta E_{net\ gain}$ with them. However, the $\Delta E_{net\ gain}$ of the minimum complexes by intercalation from the minor groove side into the cavity of dCG**AT**CG as well as of dCG**GC**CG is correlated to the experimentally determined hydrophobic term of the N10-protonated acridines, expressed in R_m values [10, 69, 81].
Thus the N10-protonated amsacrine (**1**) is the most lipophilic drug in this series and produces the highest energy gain. In this group AMSA (**3**) is the less lipophilic congener and shows the smallest energy gain in the intercalated state.

2.5.2. Calculation of the heat of formation of the complexes

The quantum mechanical heat of formation of the minimized intercalation complexes was calculated at the dinucleotide level plus the intercalator as described in chapter 3.5.4. These calculations are a great advance when compared with former studies which only compare the calculated values of the isolated bases or ligands; also while calculating charge-transfer interactions [22, 70].
Again the ranking order amsacrine > o-AMSA > AMSA for the heat of formation of the intercalation complexes from the minor groove side into dCG**AT**CG or dCG**GC**CG is found. So the correlation with the R_m values of the acridines is retained for the heat of formation calculations as was found with the force field calculations.

2.5.3. Calculation of charge-transfer interactions

Charge-transfer interactions represent another contribution to the stability of intercalation complexes [4, 22, 71]. In this study the molecule orbitals are calculated for the first time quantum mechanically combined for the complete intercalation cavity dinucleotide **plus** the intercalator (see chapter 3.5.5.) [22, 70, 72].
The HOMO is located in the purine base (adenine, guanine); in the dAT-complexes always only one adenine is involved. The pyrimidine bases (Thy, Cyt) do not participate in the charge-transfer stabilization effects. The LUMO is nearly completely located in the acridine/N11 partial structure of the 9-anilino-acridines (Fig. 16) [72, 75].
The results in short: the FMO calculations revealed, that because of a) the localization of HOMO and LUMO in different subsystems, b) of the energy difference of 5.3–5.8 eV between the FMOs, and c) because of the adequate values of the p_z-coefficients, charge – transfer interactions have a high probability of existing in the N10 protonated 9-anilino-acridine/DNA complexes by intercalation from the minor groove side [22, 72, 75]. In detail all charge-transfer data show a small preference for dGC-cavities, due to slightly higher p_z-coefficients and with 5.3–5.4 eV a smaller energy difference between the FMOs [22].

2.6. Conclusions

The DNA-binding mode of the antitumor drug amsacrine and its derivatives at the atomic level has not been solved experimentally in detail until now. No X-ray structure of an amsacrine derivative complexed with a DNA oligonucleotide exists, and only some preliminary predictions of their intercalation complexes have been reported [16–19]. Thus a detailed molecular modeling study is justified.

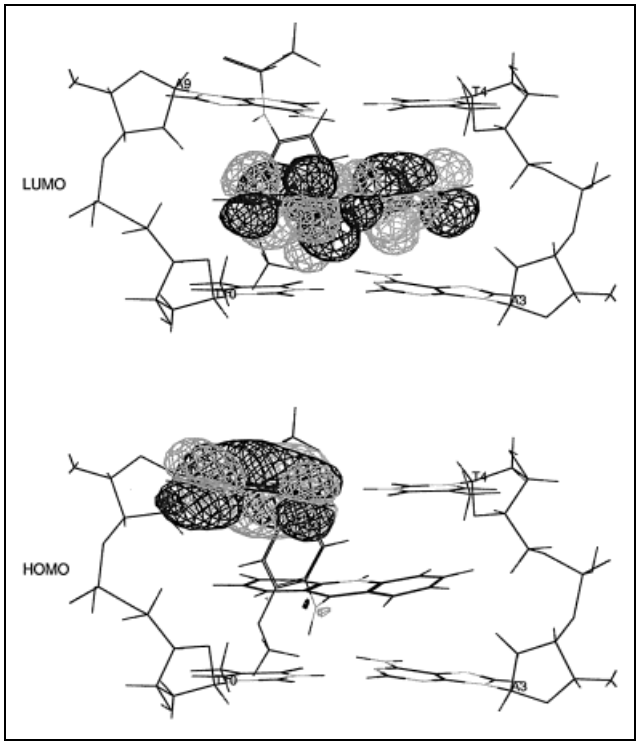

Fig. 16: Frontier molecular orbitals (FMO) of the intercalation complex of the N10 – protonated amsacrine **1** in dCG**AT**CG (as shown in Fig. 14). FMO's were calculated for the dAT cavity *plus* ligand. Upper part: The LUMO is nearly totally located in the 9-amino-acridine. Lower part: The same complex as in the upper part is shown. The HOMO is totally located in one adenine base

The interaction field analysis (GRID) favors an edge on alignment intercalation of the acridine moiety of the 9-anilino-acridines, orientated parallel to the planes of the base pairs into the enlarged DNA cavity. Our preliminary molecular dynamics simulations closing with a molecular mechanics "fine tuning" revealed that the contact of the side chain of the three drugs is throughout energetically favored in the minor groove. While intercalating from the minor groove side of the DNA-hexanucleotides the dAT-cavity is slightly favored by amsacrine (**1**) up to clearly favored by o-AMSA (**4**). The interaction of the 9-anilino-sulfonamide with the major groove is energetically favored within the dGC-cavity by amsacrine (**1**) and AMSA (**3**), whereas o-AMSA (**4**) favors generally the dAT-cavity of DNA.

A comparison of the experimental R_m values as a lipophilicity parameter revealed a reasonable correlation with the calculated $\Delta E_{net\ gain}$ values of the minimum intercalation complexes generated from the minor groove side into the cavity of dCG**AT**CG and of dCG**GC**CG. The N10-protonated amsacrine (**1**) is the most lipophilic drug in this series and produces the highest energy gain.

Moreover, the FMO calculations of the base paired dinucleotide intercalation complexes predict a small preference for the dGC-cavity. The GC-selectivity was also demonstrated by our former results with other cationic intercalators [22].

The advance of the study was

A) the detailed interaction field analysis of the DNA cavity and grooves. The information can be used to design new congeners with optimal binding properties or to choose optimal DNA-sequences for example for molecular modeling;

B) the new molecule dynamics procedure, which leads to intercalation complexes primarily due to electrostatic properties,

C) the correlation of energy terms of the force field – minimized intercalation complexes with experimental data, and

D) the quantum mechanical analysis of the whole ligand/dinucleotide complexes to get information about the stabilizing charge transfer-interactions.

After further investigations with related 9-anilino-acridines with the aim of consolidating and generalising the results, the introduced methods and the given results can be used to test the binding properties and DNA-affinity of newly designed derivatives.

3. Experimental

3.1. Minimization of the ligands (chapter 2.1.)

For the conformational analyses of compounds **1**, **3** and **4** the starting geometries from X-ray analysis were used [12, 25–27]. The bioactive, intercalating N10-protonated compounds are discussed [37, 51]. The semi-empirical quantum chemical program MOPAC 6.0 [57] was employed for minimization. Key words: AM1 VECT (or XYZ) MMOK CHARGE = 1 (last refinement: PRECISE).

3.2. Conformational analyses of the ligands (chapter 2.2.)

In the case of compounds **1** and **3** the bond C9–N11 was rotated in steps of 10° (Fig. 1). During the MOPAC minimization (see chapter 3.1) this C8a–C9–N11–C3′ torsion angle α was fixed and the remaining molecule was kept flexible [45]. For the compound **4** the studies were performed in the range α +/–20° of the minimized crystal structure.

The conformation of the sulfonamide group was investigated using the program MOPAC 6.0/AM1 [57]. As starting geometry a low energy conformation of amsacrine (**1**) was used. The torsion angle δ [C2′–C1′–N18–S19] was set to 0°, 45°, 90°, 135°, 180°, 225°, 270° and 315° (Fig. 1) and the torsion angle γ [HN18–N18–S19–C22] was set to 0°, 45°, 90°, 135° and 180°. All 40 conformations obtained were then completely minimized (chapter 3.1).

3.3. B-DNA-hexanucleotide construction and minimization (chapter 2.3.)

The interactive DNA construction procedure is described in chapter 2.3, see Fig. 4. Energy minimization of the B-DNA hexanucleotide: AMBER-force field [40], implemented in the SYBYL 5.5 program package [52]. The bases of the intercalation cavity including sugar-C1′ were fixed. The following parameters were used: nucleic acid specific AMBER charges [41], AMBER united-atom model [40, 52], 800 iterations, non-bonded reset = 2, dielectric constant = 4.0 [37, 42], distance dependent function. Hydrogens were added afterwards [53].

3.4. Interaction field analysis using the program GRID (chapter 2.4.)

GRID, version 9.02 [32, 33] was used to calculate the molecular or atomic interaction positions. Partial structures of the DNA grooves or the intercalation cavities were chosen: key word CAGE. For each groove and probe 1–4 examples of the DNA hexanucleotides with slightly different conformations were calculated.

The probes are adapted to **1** (Fig. 5, Table 1). GRID-point distance 1 Å (default). DNA phosphate groups are negatively charged. Their potassium counter cations and the hydrogens are added by default (subprogram GRIN). GRID – charges or charges from the nucleic acid – validated program AMBER [33, 41] were used.

3.5. Simulations of 9-anilino-acridine/DNA-complexes by molecular dynamics simulations, molecular mechanics and semiempirical MO calculations

For the molecular mechanics and molecular dynamics calculations the respective tools in the program package SYBYL 6.02 were used [53]. DNA hexanucleotides: Gasteiger-Hückel charges [53], no counter-ions; each phosphate group has a charge of –1. N10-protonated ligands: MOPAC 6.0-AM1/ESP-charges [35, 57]. The application of "mixed" charge models is validated by other DNA-ligand simulations in the literature [77, 78].

3.5.1. Molecular dynamics simulations (MD)

The base-paired DNA-hexanucleotides dCG**AT**CG and dCG**GC**AG with the enlarged cavity of 6.8 Å between the base pairs BP3 and BP4 (Fig. 4) were used.

As starting geometry the intercalator was set into position of about 13 Å distance related to the edge base pair – atoms of the hexanucleotide cavity

(Fig. 13, for example: distance between acridine-H4 and -H5, Fig. 1, and the major groove atoms Gua-O6 and Cyt-HN4, Fig. 6), see [38].
Starting from seven or eight with SYBYL interactively constructed starting conformations for each groove of the hexanucleotide the MD calculations were run. The following parameters were used: dielelectric constant = 4.0 [37, 39, 42], distance dependent function; non-bonded cutoff 20.0 Å; NTV-ensemble (N = constant number of n atoms in the ensemble, T, V = constant; the kinetic energy of the systems was scaled after each time interval at the given temperature).
Details of the cyclic process of the MD calculations, using SYBYL 6.02 [53]: Table 2.

3.5.2. Minimization of the complexes (molecular mechanics calculations)

Method II: SYBYL 6.02 [53], Powell conjugate gradient minimizer [36]; RMS-GRADIENT break-off criteria Δ 0.01 kcal mol^{-1} Å^{-1}, max. 1000 iterations. Non-bonded contacts: 8.0 Å (default), dielectric constant $\varepsilon = 4.0$ [37, 39, 42], distance dependent function.
B-DNA: fixed as aggregate [38]. This procedure has been approved in related molecular modeling studies of DNA complexes [21, 22, 37]. On the basis of the Tripos force field TAFF the gain of energy of the complexes is calculated according to equations **(1)**–**(3)**:
Force field [52–54]

$$E_{tot}(\text{SYBYL-TAFF})\ [\text{kcal mol}^{-1}] = E_{\text{bond stretching}} + E_{\text{angle bending}} + E_{\text{torsional}} + E_{vdW} + E_{El} + E_{1-4vdW} + E_{1-4El} + E_{\text{out of plane bending}} \quad (1)$$

which is combined to get [21, 22, 37]

$$\Delta E_{\text{net gain}} = E_{\text{tot complex}} - E_{\text{tot DNA}} - E_{\text{tot Ligand}}\ [\text{kcal mol}^{-1}]. \quad (2)$$

In the histograms given (Fig. 15) this $\Delta E_{\text{net gain}}$ is splitted into the relevant terms for the aim of comparison:

$$\Delta E_{\text{net gain}} = \Delta E_{BAT} + \Delta E_{vdW} + \Delta E_{El} + \Delta E_R\ [\text{kcal mol}^{-1}] \quad (3)$$

$$\Delta E_{BAT} = E_{\text{BAT complex}} - E_{\text{BAT DNA}} - E_{\text{BAT ligand}};$$

$$E_{BAT} = E_{\text{conformational energies}} = E_{\text{bond stretching}} + E_{\text{angle bending}} + E_{\text{tosional strain}};$$

$$\Delta E_{vdW} = \Delta E_{\text{van der Waals interactions}} = E_{\text{vdW complex}} - E_{\text{vdW DNA}} - E_{\text{vdW ligand}};$$

$$\Delta E_{El} = \Delta E_{\text{electrostatic interactions}} = E_{\text{El complex}} - E_{\text{El DNA}} - E_{\text{El ligand}};$$

$$\Delta E_R = E_{\text{R complex}} - E_{\text{R DNA}} - E_{\text{R ligand}};$$

$$E_R = E_{\text{out of plane-bending}} + E_{\text{1–4 van der Waals interactions}} + E_{\text{1–4 electrostatic interactions}}.$$

3.5.3. Comment to chapters 3.5.1 and 3.5.2

The value for non-bonded cutoff was enlarged from 8.0 Å (default value) to 20.0 Å, to enable an electrostatic attraction between ligand and DNA [38]. The value of the dielelectric constant was set to 4.0 [37, 42] in order to consider the influence of water molecules *in vivo*.
The MD method IA (Table 2) starting with conformations as pictured in Fig. 13 also leads to "outside" complexes. Some of these complexes were minimized by method II in order to compare them energetically with the intercalated complexes. Some of the total or of the former "in part" intercalation complexes were minimized according to method II and used as starting geometries for a subsequent refinement MD simulation according to method IB. This often gave rise to a complete intercalation of the "in part" intercalated complexes and gave information about relevant conformation families and low energy complexes.

3.5.4. Calculations of the heat of formation of the complexes (chapter 2.5.2)

The heat of formation ΔHf of intercalated ligand plus the surrounding dinucleotide together was calculated with MOPAC 6.0/AM1 [57]. Hydrogens were added to the 5′- and 3′-oxygens of the cut off dinucleotide producing hydroxy groups.
MOPAC key words: XYZ AM1 1SCF MMOK CHARGE = −1.

3.5.5. Calculation of charge-transfer interactions (chapter 2.5.3)

The molecular orbital (MO) calculations for analysing charge-transfer interactions of intercalated ligand plus the surrounding dinucleotide together were performed with MOPAC 6.0/AM1 [57]. The negative partial charge of the phosphate groups was neutralized by adding hydrogens to the 5′- and 3′-oxygens of the cut off dinucleotide producing hydroxy groups.
MOPAC key words: VECT AM1 1SCF MMOK CHARGE = −1.

3.6. Hardware

The programs SYBYL 6.02 and GRID were installed on VAX 4000/90 and 4000/60 machines, Sybyl 6.31 on a SGI-High Impact, the MOPAC calculations were performed on ALPHA machines DEC 3000 M300, DEC 2100 A500 MP or DEC 8400 5/300, Zentrum für Datenverarbeitung, Universität Mainz. A TRANSDEC TT401 (DEC VT220) and an IBM RISC RS 6000 computer as X-terminal were used.

References

1 Rote Liste; Rote-Liste-Sekretariat in der BPI Service GmbH: Frankfurt (1996); Fachinformationen Amsidyl® (1996)
2 Arlin, Z. A.; Sklaroff, R. B.; Gee, T. S.; Kempin, S. J.; Howard; J. Clarkson, B. D.; Young, C. W.: Cancer Res. **40**, 3304 (1980)
3 Asulacrin isethionate, clinical studies phase I: Drugs Fut. **21**, 825 (1996); Sparta Pharmaceuticals, Inc., Innovative Drug Develop. Companies, Technol. Opportunities, New York (1996)
4 Silvermann, R. B.: Medizinische Chemie, VCH Verlag Chemie, Weinheim 1995
5 Crow, R. T.; Crothers, D. M.: J. Med. Chem. **37**, 3191 (1994)
6 Minford, J.; Pommier, Y.; Filipski, J.; Kohn, K. W.; Kerrigan, D.; Mattern, M.; Michaels, S.; Schwartz, R.; Zwelling, L. A.: Biochemistry **25**, 9 (1986)
7 Insaf, S. S.; Danks, M. K.; Witiak, D. T.: Curr. Med. Chem. **3**, 437 (1996)
8 Cain, B. F.; Wilson, W. R.; Baguley, B. C.: Mol. Pharmacol. **12**, 1027 (1976)
9 Baguley, B. C.; Denny, W. A.; Atwell, G. J.; Cain, B. F.: J. Med. Chem. **24**, 170 (1981)
10 Baguley, B. C.; Nash, R.: Eur. J. Cancer **17**, 671 (1981)
11 Denny, W. A.; Cain, B. F.: J. Med. Chem. **21**, 430 (1978)
12 Abraham, Z. H. L.; Cutbush, S. D.; Kuroda, R.; Neidle, S.; Acheson, R. M.; Taylor, G. N.: J. Chem. Soc., Perkin Trans. II, 461 (1985)
13 Denny, W. A.; Cain, B. F.; Atwell, G. J.; Hansch, C.; Panthananickal, A.; Leo, A.: J. Med. Chem. 25, 276 (1982)
14 Cain, B. F.; Seelye, R. N.; Atwell, G. J.: J. Med. Chem. **17**, 922 (1974)
15 Rewcastle, G. W.; Atwell, G. J.; Chambers, D.; Baguley, B. C.; Denny, W. A.: J. Med. Chem. **29**, 472 (1986)
16 Neidle, S.; Abraham, Z.: Crit. Rev. Biochem. **7**, 73 (1984)
17 Neidle, S.; Abraham, Z. H. L.; Collier, D. A.; Islam, S.A; in: New Avenues in Developmental Cancer Chemotherapy, pp. 83, Academic Press Inc., London 1987
18 Neidle, S.; in: Neidle, S. (Ed.): Topics in Nucleic Acid Structures, pp. 177, The Macmillan Press Ltd., London 1982
19 Chen, K.-X.; Gresh, N.; Pullman, B.: Nucleic Acids Res. **16**, 3061 (1988)
20 Pindur, U.; Haber, M.; Sattler, K., J.: Chem. Edu. **4**, 263 (1993)
21 Rehn, C.; Pindur, U.: Monatsh. Chem. **127**, 631 (1996)
22 Rehn, C.; Pindur, U.: Monatsh. Chem. **127**, 645 (1996)
23 Karle, J. M.; Cysyk, R. L.; Karle, I. L.: Acta Cryst. **B36** (1980). 3012
24 Baguley, B. C.; Denny, W. A.; Atwell, G. J.; Finlay, G. J.; Rewcastle, G. W.; Twigden, S. J.; Wilson, W. R.: Cancer Res. **44** (1984). 3245
25 Buckleton, J. S.; Clark, G. R.: Acta Cryst. **C48**, 1085 (1992)
26 Hall, D.; Swann, D. A.; Waters, T. N.: J. Chem. Soc., Perkin Trans. II, 1334 (1974)
27 Neidle, S.; Webster, G. D.; Baguley, B. C.; Denny, W. A.: Biochem. Pharmacol. **35**, 3915 (1986)
28 Wang, A. H.-J.; Gao, Y.-G., Liaw, Y.-C.; Li, Y.-K.: Biochemistry **30**, 3812 (1991)
29 Jain, S. C.; Sobell, H. M.: J. Biomol. Struct. Dyn. **1**, 1179 (1984)
30 Lipscomb, L. A.; Peek, M. E.; Zhou, F. X.; Bertrand, J. A.; Vanderveer, D.; Williams, L. D.: Biochemistry **33**, 3649 (1994)
31 Höltje, H.-D.; Folkers, G.; in: Mannhold, R.; Kubinyi, H.; Timmerman, H. (Eds.): Molecular Modeling – Basic Principles and Applications, Vol. 5, VCH Verlagsgesellschaft mbH, Weinheim 1996
32 Goodford, P. J.: J. Med. Chem. **28**, 849 (1985)
33 GRID, Vers. 9.02, Molecular Discovery Ltd, England, Oxford 1991
34 CONNOLLY, QCPE 429; Indiana University, Bloomington, Indiana, USA 1992
35 Besler, B.; Merz, K. M.; Kollman, P. A.: J. Comp. Chem. **4**, 431 (1990)
36 Kunz, R. W.; in: Elschenbroich, C.; Hensel, F.; Hopf, H. (Eds.): Molecular Modeling für Anwender: Anwendung von Kraftfeld- und MO-Methoden in der organischen Chemie, Teubner, Stuttgart 1991
37 Neidle, S.; in: Beddell, C. R. (Ed.): The design of drugs to macromolecular targets, pp. 173, J. Wiley & Sohns Ltd., New York 1992
38 Rodger, A.; Taylor, S.; Adlam, G.; Blagbrough, I. S.; Haworth, I. S.: Bioorg. Med. Chem. **3**, 861 (1995)
39 Orozko, M.; Laughton, C. A.; Herzyk, P.; Neidle, S.: J. Biomol. Struct. Dyn. **8**, 359 (1990)
40 AMBER 4.0, School of Pharmacy, Department of Pharmaceutical Chemistry, San Francisco, California, USA 1991
41 Weiner, S. J.; Kollman, P. A.; Case, D. A.; Singh, U. C.; Ghio, C.; Alagona, G.; Profeta, S.; Weiner, P.: J. Am. Chem. Soc. **106**, 765 (1984)
42 Furet, P; Caravatti, G.; Lydon, N.; Priestle, J. P.; Sowadski, J. M.; Trinks, U.; Traxler, P.: J. Comput. – Aided Mol. Des. **9**, 465 (1995)
43 Souhassou, M.; Aubry, A.; Boussard, G.; Marraud, M.: Angew. Chemie, Int. Ed. Engl. **25**, 447 (1986)
44 D. Schollmeyer; Institute of Organic Chemistry, University of Mainz, personal communication
45 Fischer, G.; Pindur, U.: Monatsh. Chem. **126**, 303 (1995)

46 Neidle, S.; in: Horn; DeRanter (Eds.): X-ray Crystallography and Drug Action, pp. 129, Clarendon Press, Oxford 1984
47 Bernstein, F. C.; Koetzle, T. F.; Williams, G. J. B.; Meyer, E. F.; Brice, M. D.; Rodgers, J. R.; Kennard, O.; Shikanouchi, T.; Tasumi, M.: J. Mol. Biol. **112**, 535 (1977).
48 Schneider, R.; Cohen, D.; Berman, H. M.: Biopolymers **32**, 725 (1992)
49 Frederick, C. A.; Williams, L. D.; Ughetto, G.; van der Marel, G. A.; van Boom, J. H.; Rich, A.; Wang, A. H.-J.: Biochemistry **29**, 2538 (1990)
50 Pindur, U.; Fischer, G.: Curr. Med. Chem. **3**, 325 (1996)
51 Wilson, W. R.; Baguley, B. C.; Wakelin, L. P. G.; Waring, M. J.: Mol. Pharmacol. **20**, 404 (1981)
52 SYBYL 5.5, Tripos Assoc. Inc., St. Louis, USA 1992
53 SYBYL 6.02, Tripos Assoc. Inc., St. Louis, USA 1993
54 SYBYL 6.31, Tripos Assoc. Inc., St. Louis, USA 1996.
55 Allen, F. H.; Bellard, S.; Brice, M. D.; Cartwright, B. A., Doubleday, A.; Higgs, H.; Hummelink, T.; Hummelink-Peters, B. G.; Kennard, O.; Motherwell, W. D. S.; Rodgers, J. R.; Watson, D. G.: Acta Cryst. **B35**, 2331 (1979)
56 Fantucci, P.; Marino, T.; Russo, N.; Villa, A. M.: J. Comput.-Aided Mol. Des. **9**, 425 (1995)
57 MOPAC 6.0, QCPE 455; Steward, J. J. P.: J. Comput.-Aided Mol. Des. **4**, 1 (1990)
58 Hansen, M.; Lee, S.-J.; Cassady, J. M.; Hurley, L. H.: J. Am. Chem. Soc. **118**, 5553 (1996)
59 Lown, J. W.; Hanstock, C. C.; Bradley, R. D.; Scraba, D. G.: Molec. Pharmacol. **25**, 178 (1984)
60 Parks, M. E.; Baird, E. E.; Dervan, P. B.: J. Am. Chem. Soc. **118**, 6147 (1996)
61 Stubbe, J.; Kozarich, J. W.; Wu, W.; Vanderwall, D. E.: Acc. Chem. Res. **29**, 322 (1996)
62 Sakore, T. D.; Reddy, B. S.; Sobell, H. M.; J. Mol. Biol. **135**, 763 (1979)
63 Saenger, W.; in: Principles of nucleic acid structure, Springer-Verlag/ Springer Advanced Texts in Chemistry, New York 1983
64 Denny, W. A.; Wakelin, L. P. G.: Cancer Res. **46**, 1717 (1986)
65 Rene, B.; Fosse, P.; Khelifa, T.; Jacquemin-Sablon, A.; Bailly, C.: Mol. Pharmacol. **49**, 343 (1996)
66 Frederick, C. A.; Grable, J.; Melia, M.; Samudzi, C.; Jen-Jacobson, L.; Wang, B.-C.; Greene, P.; Boyer, H. W.; Rosenberg, J. M.: Nature **309**, 327 (1984)
67 Weiner, P. K.; Langridge, R.; Blaney, J. M.; Schaefer, R.; Kollman, P. A.: Proc. Natl. Acad. Sci. USA **79**, 3754 (1982)
68 MacDonald, T. L.; Lehnert, E. K.; Loper, J. T.; Chow, K.-C.; Ross, W. E.; in: Potmesil, M.; Kohn, K. W. (Eds.): DNA, Topoisomerase, pp. 199, Cancer Oxford Univ. Press, New York 1991
69 Atwell, G. J.; Rewcastle, G. W.; Denny, W. A.; Cain, B. F.; Baguley, B. C.: J. Med. Chem. **27**, 367 (1984)
70 Patterson, S. E.; Coxon, J. M.; Strekowski, L.: Bioorg. Medicin. Chem. **5**, 277–281 (1997)
71 Schellmann, J. A.; Reese, H. R.: Biopolymers **39**, 161 (1995)
72 Höltje, H.–D.; Jendretzki, U. K.: Arch. Pharm. **328**, 577 (1995)
73 Kennard, O.; Hunter, W. N.: Angew. Chem. **103**, 1280 (1991)
74 Coll, M.; Frederick, C. A.; Wang, A. H.-J.; Rich, A.: Proc. Natl. Acad. Sci. USA **84**, 8385 (1987)
75 Mayoh, B.; Prout, C. K.: J. Chem. Soc., Perkin Trans. II, 1072 (1972)
76 Kimura, M.; Kato, A.; Okabayashi, I.: J. Heterocyc. Chem. **29**, 73 (1992)
77 Molina, A.; Vaquero, J. J.; Garcia-Navio, J. L.; Alvarez-Builla, J.; de Pascual-Teresa, B.; Gago, F.; Rodrigo, M. M.; Ballesteros, M.: J. Org-Chem. **16**, 5587 (1996)
78 Elcock, A. H.; Rodger, A.; Richards, W. G.: Biopolymeres **39**, 309 (1996)
79 ACRAMS, ACRMSA, ACRMSB (II), CIRTIG (III), CIRTIG01, DIRMIA, DIRMOG (III), FEKYEZ (III), FUJWIQ, HOMSAN, HPAFMS, JENGIS, KEZYET (II), KEZYIX, KEZYOD, KOYVID (III), MESTZC, MPMSAB, MPSAHT10 (II), MSACTZ10, MSULFN, NADLIN, SOTALC, SUDGON, WINWUL, YABGUD, YABMIX (II). Without numbers in brackets: group I; JENGIS: two independent molecules in the asymmetric unit
80 Abbreviations used: e.g. dCG**CG**CG = DNA hexanucleotide d(CpGp**CpG**pCpG)$_2$, rCG = RNA dinucleotide r(CpG)$_2$, A/T = A*T or T*A; BP = base pair; BP4 = base pair 4 of a DNA hexanucleotide; Pu = purine, Py = pyrimidine; Gua-HN2 = free hydrogen of Gua-N2, which is not involved in the hydrogen bonds of the base pairing.
81 Reversed phase chromatography, cationic 9-anilino-acridines; $R_m = (\log (1 - R_f)/R_f)$ [10, 13, 69]

Received March 30, 1998
Accepted June 23, 1998

Prof. Dr. U. Pindur
Institute of Pharmacy
Department of Chemistry and Pharmacy
University of Mainz
Saarstr. 21
D-55099 Mainz
pindur@mail.uni-mainz.de

Institut für Pharmazeutische Chemie der Martin-Luther-Universität, Halle, Germany

Synthese von substituierten Benzoylacrylsäuren als potentielle Hemmer der Phospholipase A_2

P. Nuhn, A. Herrmann und M. Radman

Langkettige Alkylbenzole wurden mit Maleinsäureanhydrid und substituierten Maleinsäureanhydriden zu Benzoylacrylsäuren acyliert, die auf eine Hemmung der Phospholipase A_2 untersucht wurden. Das Isomerengemisch (Z/E) wurde NMR-spektroskopisch ermittelt. Einige Benzoylacrylsäuren cyclisierten zu Hydroxybutenoliden.

Synthesis of substituted benzoyl acrylic acids as potential inhibitors of phospholipase A_2

Long chain alkylbenzenes were acylated with maleic anhydride and substituted maleic anhydrides. The resulting benzoyl acrylic acids were tested on phospholipase A_2. The isomeric ratio (Z/E) of the benzoyl acrylic acids was estimated by NMR spectroscopy. A few acrylic acids cyclized to hydroxybutenolids.